ELECTRON TRANSFER DISSOCIATION OF A MELECTIN PEPTIDE: CORRELATING THE PRECURSOR ION STRUCTURE WITH PEPTIDE BACKBONE DISSOCIATIONS

Christopher L. Moss[a1], Thomas W. Chung[a2], Václav Čeřovský[b] and František Tureček[a3,*]

[a] *Department of Chemistry, Bagley Hall, Box 351700, University of Washington, Seattle, WA 98195-1700, USA; e-mail: [1] cmoss@u.washington.edu, [2] atchung@uw.edu, [3] turecek@chem.washington.edu*

[b] *Institute of Organic Chemistry and Biochemistry, Academy of Sciences of the Czech Republic, v.v.i., Flemingovo nám. 2, 166 10 Prague 6, Czech Republic; e-mail: cerovsky@uochb.cas.cz*

Received January 30, 2011
Accepted March 4, 2011
Published online March 17, 2011

Dedicated to Dr. Zdeněk Havlas on the occasion of his 60th birthday.

Electron transfer dissociation (ETD) of doubly and triply charged ions from the amphipathic N-terminal decapeptide GFLSILKKVL-NH_2 segment of melectin gave different distributions of fragment ions. The triply charged ions generated extensive series of fragment ions of ***c*** and ***z*** type that covered the entire sequence from both the N and C termini. In contrast, electron transfer to the doubly charged ions caused backbone cleavages that occurred at residues close to the N and C termini. Attachment of a free low-energy electron to the doubly charged ions caused primary dissociations close to the N and C termini that were followed by consecutive dissociations of ***z*** ions. The structure of gaseous doubly charged ions from the melectin peptide was elucidated by a combination of exhaustive conformational search by force-field molecular dynamics, large-scale gradient optimization using the semiempirical PM6 method, and density functional theory single-point energy and gradient optimization calculations. The most stable doubly charged ions were found to be protonated at the lysine ε-amino groups and have globular conformations. The backbone cleavages in ETD correlated with the electronic structure of cation-radicals produced by electron attachment to the most stable conformers. The charged lysine ammonium groups direct the incoming electron to the π* orbitals at the proximate amide groups at Phe, Leu, Lys and Val residues that show the highest spin densities. Electron attachment at these amide groups weakens the N–C_α bonds between the Phe-Leu, Leu-Ser, Lys-Lys and Lys-Val residues and causes backbone dissociations.

Keywords: Mass spectrometry; Peptides; Ab initio calculations.

doi:10.1135/cccc2011025

Electron based methods of bioanalytical mass spectrometry, which are collectively referred to as ExD, represent useful modern tools for peptide and protein identification and sequencing[1]. In the electron transfer dissociation method (ETD)[2], multiply protonated peptide ions are allowed to react with anion electron donors to reduce the peptide ion by attachment of one or more electrons. This converts the stable even-electron peptide ions to labile cation-radicals that dissociate through multiple reaction channels. The analytically most useful dissociations of charge-reduced peptide cation-radicals comprise backbone bond breaks that occur specifically between the amide nitrogen atoms and the adjacent C_α atoms, N–C_α bond cleavages for short (Scheme 1). These backbone dissociations produce series of N-terminal fragments (*c* ions) and C-terminal fragments (*z* ions) that carry information about the amino acid sequence in the peptide. Ideally, a series of $n - 1$ *c* or *z* ions from a peptide consisting of *n* amino acid residues provides a complete amino acid sequence except for isomeric leucine and isoleucine resi-

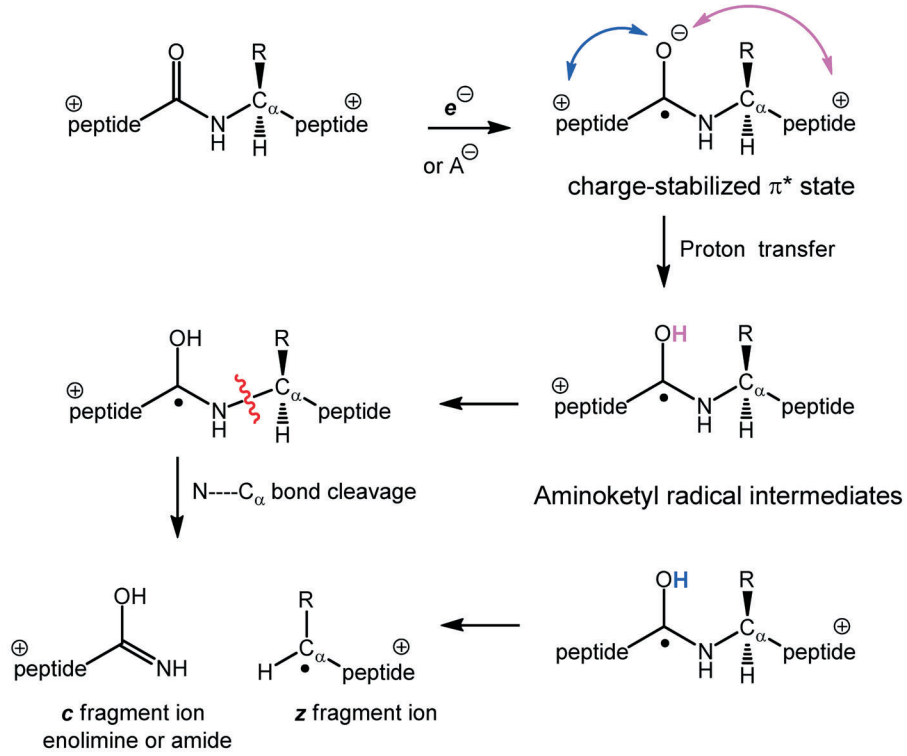

SCHEME 1

dues. Hence, it is desirable that the backbone dissociations be nonspecific to the nature of the N–C_α bonds between the different amino acid residues to cleave these bonds with comparable probability and form the highest number of sequence fragments. The preferential N–C_α bond cleavages in peptide cation-radicals is due to their electronic structure that has been elucidated for model di- through pentapeptides[3]. It has been found that electron attachment results in a very significant lowering of N–C_α bond dissociation energies as well as energy barriers in the relevant transition states[4,5]. The calculated transition state energies typically range within 7–50 kJ/mol [6], which is comparable to the barrier for the chair-twist boat ring flipping in cyclohexane (45–48 kJ/mol)[7–9]. In fact, some bond breaking reactions in peptide radicals have been reported to have rate determining steps due to conformational transformations of the peptide backbone and side chains[10,11].

Conformational effects have been noted in electron capture dissociation (ECD) of peptide and protein ions. McLafferty and coworkers[12,13] and others[14] studied ECD of various charge states of gas-phase ubiquitin ions and correlated the observed backbone dissociations with the presumed ion tertiary structure. Temperature effects[15], substitution of D for L amino acid residues[16], and peptide sequence[17] have been shown to influence backbone dissociations of peptide ions upon electron capture. There have been a few computational studies of structure effects on electron attachment and dissociation that addressed peptide ion secondary structures[18–20].

One of the fundamental questions of ExD concerns the effects of charge sites on backbone and other dissociations of charge-reduced peptide ions. Peptide charging by multiple protonation in electrospray is presumed to occur by placing the protons on the most basic sites in the molecule or ion. With tryptic peptides in particular, the C-terminal Lys or Arg residues are practically always protonated. The other protons occupy other basic residues, e.g., the His imidazole ring, or the N-terminal amino group which have intrinsic basicities that exceed those of peptide amide groups. However, intramolecular hydrogen bonding can overwhelm the differences in intrinsic group basicities, and in such a case the protonation sites also depend on the ion secondary structure. These effects introduce substantial uncertainty as to the valence bond structure (protonation sites) and conformation (secondary structure) of gas-phase peptide ions that are not amenable to experimental analysis. Therefore, the structure assignment relies entirely or to a large extent on computational analysis.

In an effort to achieve some control over the peptide ion structure, we selected an N-terminal decapeptide segment of melectin[21] for this model

study. This peptide (GFLSILKKVL-NH_2) contains two lysine residues which are presumably protonated in the doubly charged gas phase ion, defining its valence-bond structure. Furthermore, the melectin peptide has been reported to display substantial helicity in solution when probed by circular dichroism measurements[21]. We wish to explore if the presumed valence-bond isomers, as well as conformers, are present in the gas phase. Another topic of interest is the effect of the gas-phase ion structure on backbone dissociations following electron transfer.

RESULTS

Electrospray ionization of the melectin peptide provided the triply protonated $(M + 3H)^{3+}$ (*m/z* 372.9) and doubly protonated $(M + 2H)^{2+}$ (*m/z* 558.9) ions as the dominant species in a 54:46 ratio of relative intensities. The singly protonated $(M + H)^+$ ion at *m/z* 1116.7 was also present but weak (~1% of multiply charged ion intensities). The doubly and triply charged ions were mass-selected for ETD measurements. The ETD mass spectra of the $(M + 2H)^{2+}$ precursor ions showed charge reduction conversions that depended on the ion-ion interaction time which was varied from 50 to 999 ms. The electron transfer efficiency was expressed according to Eq. (*1*), where I_k are the charge-reduced ion intensities and I_P is the intensity of the residual doubly charged precursor ion.

$$\%E = \frac{100\sum_k I_k}{\sum_k I_k + I_P} \qquad (1)$$

Figure 1a shows that the electron transfer efficiency increased with the ion-ion interaction time, reaching 62% at 300 ms. The logarithmic plot of (100 – *E*) (Fig. 1b) showed a linear dependence on time (r^2 = 0.9996), indicating that the electron transfer was a pseudofirst order reaction occurring at a large excess of the electron donor reagent. ETD of the triply charged precursor ion was more efficient, reaching 94% conversion to lower charge states after 300 ms ion-ion interaction time. The 300 ms ETD spectra will be discussed.

The ETD mass spectrum of the doubly charged precursor shows a series of N-terminal (*c* type) and C-terminal (*z* type) fragment ions (Fig. 2a). For peptide fragment ion nomenclature see ref.[22]. The *z*-ion series starts at z_5, which is formed by cleavage of the N–C_α bond between the Ile and Leu residues. The main fragments of this series are the z_8 and z_7 ions that arise by

N–C_α bond cleavages between the Phe and Leu, and Leu and Ser residues, respectively. The ***c*** ion series starts at c_7 which is the most abundant ion of this series and is due to N–C_α bond cleavage between the Lys residues. The c_8 and c_9 fragment ions are also formed, corresponding to N–C_α bond cleavages between the Lys and Val, and Val and Leu residues, respectively.

The ECD mass spectrum of the doubly charged precursor ion showed a series of *c* and *z* fragments (Fig. 2b) with accurate *m/z* values that matched the theoretical ones within 0.4 ± 0.3 millimass units and confirmed the

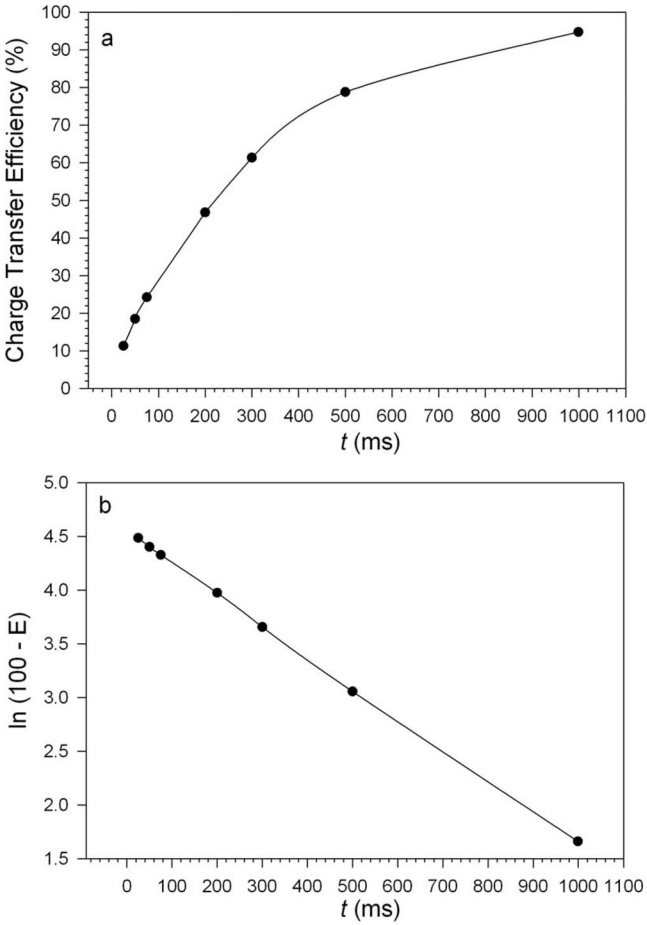

FIG. 1
Time dependence of ETD product yield. a Plot of ETD efficiency (*E*, %) according to Eq. (*1*). b Plot of ln (100 – *E*)

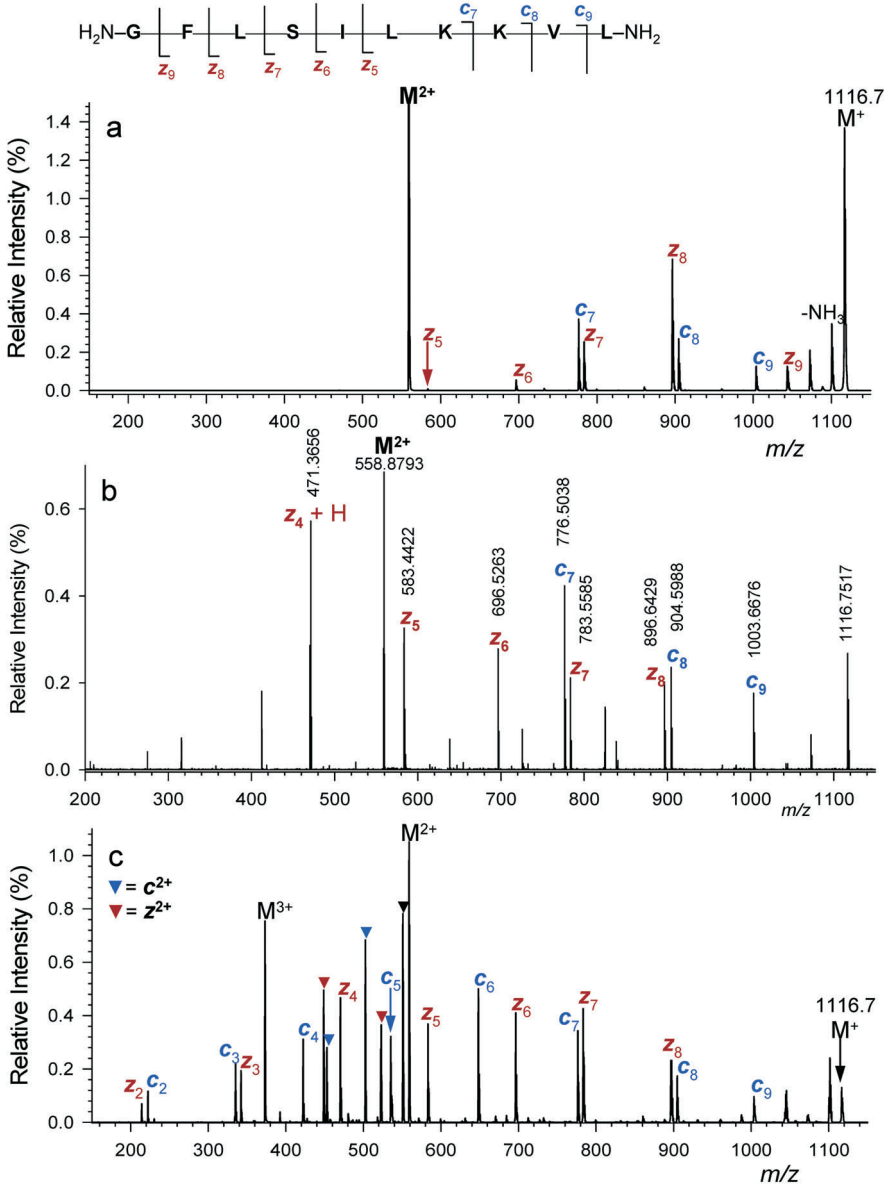

FIG. 2

a ETD mass spectrum at 300 ms ion-ion interaction time of doubly protonated melectin peptide at *m/z* 558.9. b ECD mass spectrum at 500 ms ion-ion interaction time of doubly protonated melectin peptide at *m/z* 558.9. c ETD mass spectrum, of triply protonated melectin peptide at *m/z* 372.9; doubly charged fragment ions are denoted by inverted color triangles

fragment assignments. The ECD spectrum showed the same ordering of c_7–c_9 ion relative intensities as did the ETD mass spectrum. Differences were observed for the *z* ions that formed a series of peaks of an increasing relative intensity from z_8 through z_5. The z_4 fragment appeared exclusively as a z_4 + H ion, as confirmed by accurate mass measurement (Fig. 2b). The differences in the *z* ion relative intensities in the ETD and ECD mass spectra can be assigned to a higher excitation upon capture of free electron that drives consecutive dissociations of *z* ions, thus increasing the relative intensities of the smaller fragments.

The ETD mass spectrum of the triply charged precursor (*m/z* 372.9) showed extensive series of both *z*-type fragments (z_2 at *m/z* 214 through z_9 at *m/z* 1043) and *c*-type fragments (c_2 at *m/z* 222 through c_9 at *m/z* 1003, Fig. 2c). The relative intensities of both fragment series showed smooth distributions peaking at z_4 and c_6, respectively, with a minor dip for z_5 and c_5 ions. The latter are complementary fragments from N–C_α bond cleavage between the Ile and Leu residues. Doubly charged fragments are represented by *m/z* 392.3, 448.8 and 522.4 for z_7^{2+} through z_9^{2+}, respectively, and *m/z* 452.8 and 502.3 for c_8^{2+} and c_9^{2+}, respectively.

DISCUSSION

The ETD mass spectrum of the doubly protonated melectin peptide shows preferential N–C_α bond cleavages in the region of the F-L-S and K-K-V residues. In contrast, ETD of the triply protonated ion tends to cleave bonds towards the center of the peptide chain. We now address the structures of the doubly charged ions and their relationship to the observed dissociations. The presumed protonation sites in the melectin peptide are the Lys ε-amino groups. Replica exchange molecular dynamics followed by PM6 reoptimization yielded several conformers that were closely spaced in energy. However, B3LYP single-point energy calculations on the PM6 optimized geometries resulted in much greater energy differences and a very different ranking of conformer relative energies for several lowest energy structures identified by PM6 (Table I). The B3LYP relative energies did not depend on the basis set used and so only the 6-311+G(2d,p) data are shown in Table I. B3LYP failed to optimize peptide ion geometries, presumably because of long-range interactions in these peptide ions. We reasoned that DFT methods that include long-range corrections might be suitable for geometry optimization and thus we selected the two most stable conformers according to single-point energies for reoptimization with cam-B3LYP/6-31+G(d,p)[23] to yield structures $\mathbf{2a}^{2+}$ and $\mathbf{3a}^{2+}$ (Fig. 3). Interestingly, the relative energies

of cam-B3LYP optimized $\mathbf{2a}^{2+}$ and $\mathbf{3a}^{2+}$ were practically the same as those from single point B3LYP calculations on PM6 optimized structures $\mathbf{2}^{2+}$ and $\mathbf{3}^{2+}$ (Table I). However, the size of these systems (178 atoms) prevented us from obtaining optimized structures for a large number of peptide ion conformers, and thus the lowest-energy structure corresponding to a global energy minimum of this protonation tautomer could not be assigned with certainty. All low-energy conformers showed a similar pattern of intramolecular hydrogen bonding in which the protonated Lys ε-ammonium

TABLE I
Relative energies of conformers of doubly protonated melectin decapeptide

Ion conformer	Relative energy, kJ/mol		
	PM6	B3LYP[a]/ 6-311+G(2d,p)	cam-B3LYP[b]/ 6-31+G(d,p)
$\mathbf{1}^{2+}$	0	0	0
$\mathbf{2}^{2+}$	16	–96	–96
$\mathbf{3}^{2+}$	6	–82	–81
$\mathbf{4}^{2+}$	12	–79	–
$\mathbf{5}^{2+}$	13	–14	–
$\mathbf{6}^{2+}$	15	–46	–
$\mathbf{7}^{2+}$	15	–49	–48
$\mathbf{8}^{2+}$	47	18	–

[a] Based on single-point energy calculations. [b] Optimized structures at the 10^{-5} a.u. (0.026 kJ/mol) limit.

TABLE II
NPA atomic spin densities at amide groups[a]

Ion	Atomic spin density									
	H_2N–G	F	L	S	I	L	K	K	V	L–NH_2
$\mathbf{1}^{\bullet+}$	0.01	0.03	0.18	0.02	0.04	0.14	**0.27**	0.01	0.007	0.06
$\mathbf{2}^{\bullet+}$	**0.21**	0.006	0.11	0.02	0.05	0.12	0.16	0.002	0.02	0.003
$\mathbf{3}^{\bullet+}$	0.08	0.12	0.11	0.05	0.008	0.05	**0.21**	0.01	0.001	0.04

[a] Sums of NPA atomic spin densities on C, O and N atoms in the corresponding amide groups.

groups pointed to the opposite regions of the peptide structure. This arrangement is understandable, because it minimizes Coulomb repulsion between the charged groups. For illustration, three low energy structures preferred either by PM6 ($\mathbf{1}^{2+}$) or B3LYP and cam-B3LYP ($\mathbf{2a}^{2+}$ and $\mathbf{3a}^{2+}$) are presented in Fig. 3.

Structure $\mathbf{1}^{2+}$ shows the Lys-7 ammonium hydrogen-bonded to the Phe, Lys-7 and Val amide carbonyls. The Lys-8 ammonium is H-bonded to the Ser, Ile and Leu-6 amide carbonyls. Structures $\mathbf{2}^{2+}$ and $\mathbf{2a}^{2+}$ show the Lys-7 ammonium hydrogen-bonded to the Ser OH, Lys-7, Val and C-terminal amide carbonyls. The Lys-8 ammonium is H-bonded to the Ser, Ile and Leu-6 amide carbonyls. Structures $\mathbf{3}^{2+}$ and $\mathbf{3a}^{2+}$ have the Lys-7 ammonium hydrogen-bonded to the Phe, Lys-7, Val and C-terminal amide carbonyls. The Lys-8 ammonium in $\mathbf{3}^{2+}$ and $\mathbf{3a}^{2+}$ is H-bonded to the Ser, Ile and Leu-6 amide carbonyls.

Other tautomers were also investigated in which one proton was placed on the N-terminal amino group and the other on the Lys-7 ε-amino group,

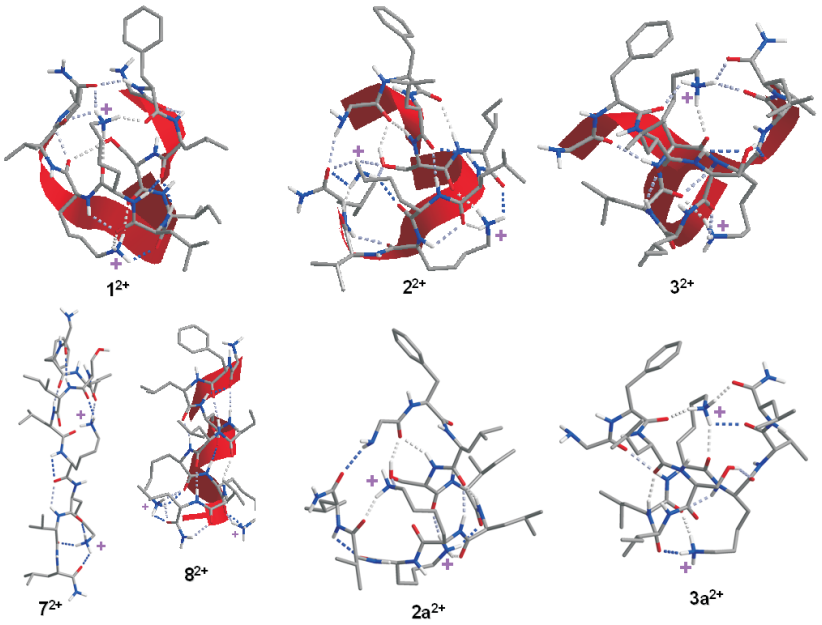

FIG. 3
Optimized structures of gas-phase conformers of doubly protonated melectin decapeptide. Structures $\mathbf{1}^{2+}$–$\mathbf{3}^{2+}$ and $\mathbf{8}^{2+}$ are from PM6 optimizations, structures $\mathbf{2}^{2+}$, $\mathbf{3a}^{2+}$ and $\mathbf{7}^{2+}$ are from cam-B3LYP/6-31+G(d,p) optimizations

and the conformational space was mapped by REMD. However, PM6 optimization of such conformers resulted in a spontaneous proton shift to the neutral Lys ε-amino group. This indicates that Lys protonation is energetically favored. In addition, helical conformers ($\mathbf{7}^{2+}$ and $\mathbf{8}^{2+}$) were optimized by PM6, then their single-point energies were calculated by B3LYP, and the geometry of $\mathbf{7}^{2+}$ was reoptimized with cam-B3LYP. All these calculations placed the energies of structures $\mathbf{7}^{2+}$ and $\mathbf{8}^{2+}$ above those for the pertinent most stable conformers $\mathbf{2}^{2+}$/$\mathbf{2a}^{2+}$ and $\mathbf{3}^{2+}$/$\mathbf{3a}^{2+}$ (Table I). Hence, we conclude that the doubly protonated melectin peptide prefers globular conformations in the gas phase.

Vertical electron attachment to ions $\mathbf{1}^{2+}$–$\mathbf{3}^{2+}$ gave cation-radicals that are represented by the singly-occupied molecular orbital (SOMO) of the ground electronic state of $\mathbf{1}^{\bullet+}$ (SOMO, Fig. 4). This shows substantial delocalization of the unpaired electron density over the amide groups at Lys-7, Leu-3 and Leu-6. Likewise, vertical electron attachment to $\mathbf{2}^{2+}$ and $\mathbf{3}^{2+}$ formed high spin density regions at Gly and Lys-6, and Phe and Lys-7, respectively. The lowest virtual molecular orbitals (MO) of the charge-reduced cation-radicals

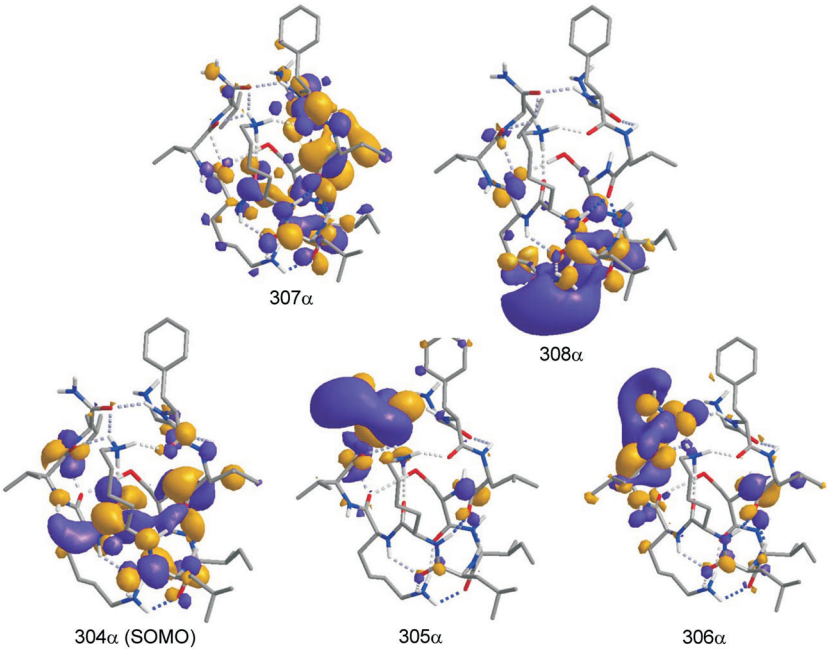

FIG. 4
UB3LYP/6-31++G(2d,p) alpha molecular orbitals of the cation-radical from vertical electron attachment to melectin decapeptide ion $\mathbf{1}^{2+}$

show significant contributions of π* orbitals located at amide groups close to the C-terminus (MO 305α and 306α) or along the backbone. We did not carry out excited-state calculations for these large systems, and so the energies of low-lying excited states including ammonium Rydbergs could not be evaluated. The vertical recombination energy of $\mathbf{1}^{2+}$ was calculated by B3LYP/6-31++G(2d,p) as 4.0 eV. This is a rather low value for a doubly charged decapeptide ion, considering the distance of the charged ammonium groups in $\mathbf{1}^{2+}$ (8.8 Å) and the associated Coulomb repulsion energy (1.6 eV) which is released upon electron attachment.

We note that B3LYP is likely to overestimate electron delocalization in peptide cation-radicals because of the electron self-interaction problem[23] and the charge-transfer characteristics of electron excitation to low-lying excited states[5]. Although a systematic treatment of this problem is beyond the scope of this work, we attempted to use long-range corrected hybrid density functionals to describe the electronic structure of vertically reduced $\mathbf{1}^{\bullet+}$ and $\mathbf{2}^{\bullet+}$. A single point calculation of $\mathbf{2}^{\bullet+}$ with the recently reported ωB97x functional[24] and the 6-31++G(2d,p) basis set gave atomic spin densities that showed a large degree of spin polarization by Mulliken population analysis (up to –0.35) and incorrect total charges for the occupied α (–3.72) and β orbitals (–2.36) when evaluated by Natural Population analysis of the wave functions. This obvious failure of ωB97x means that the question of electron distribution in these large peptide cation-radicals remains unresolved.

B3LYP calculations on the vertically reduced ions pointed to an accumulation of spin density in amide groups that are proximate to the charge-carrying Lys-6 and Lys-7 ammonium groups. The spin densities (Table II) correlate with the preferential cleavages of N–C_α bonds observed in the ETD mass spectrum of the doubly charged melectin peptide ion. Thus, formation of the $\boldsymbol{c_7}$ fragment can be promoted by electron attachment to the Lys-6 or Lys-7 amide groups, and formation of the $\boldsymbol{z_8}$ ion can be promoted by electron attachment to the Phe or Leu-3 amide groups. Conversely, amide groups that receive little or no spin density upon electron attachment (Ser, Ile) show low propensity for dissociation of the pertinent N–C_α bond and formation of the $\boldsymbol{z_5}$ or $\boldsymbol{z_6}$ fragments. According to the Utah-Washington model of ExD[25] (Scheme 1), electron attachment to the amide group produces a transient superbasic anion radical that can transfer a proton to form an aminoketyl radical. The latter undergoes a very facile N–C_α bond dissociation to form a complex of the incipient $\boldsymbol{c}$ and $\boldsymbol{z}$ fragments that eventually dissociates. Zwitterionic structures in charge-reduced peptide cation-radicals have recently been indicated as local energy minima

by analysis of electronic states of several pentapeptides[26,27]. Alternatively, the accumulation of odd-electron density in the amide group can promote N–C_α bond dissociation to form an enol imidate anion which is also very basic and can abstract a proton from the complementary fragment to form an amide[28,29]. A recent analysis of the energetic of N–C_α bond dissociations in a pentapeptide ion showed lower activation energy for aminoketyl groups as compared to amide radical anions[26]. However, whether this finding can be extended to general peptides will require further study.

We note that a previous study of ECD of Trp cage peptide attempted to correlate the observed fragment intensities with hydrogen bonds among neutral groups in the ion[18]. The previous authors used the Gromacs molecular dynamics program to obtain a set of conformations and made an ad hoc assumption regarding the protonation sites. In our study, we investigated tautomers in which the protonation sites appear to be well established as local energy minima by full structure optimization and we used a higher level of theory to find low-energy conformers. The correlation we find for the melectin peptide unambiguously points to the role of the charged groups in steering the electron to the π^* orbitals at the proximate amide groups. These results are consistent with the current models of ExD of peptide ions which are based on electronic structure theory.

CONCLUSIONS

Molecular dynamics, semiempirical and DFT calculations prefer globular conformers for doubly protonated ions of the amphipathic decapeptide from melectin in the gas phase. Electron transfer to the triply protonated melectin peptide results in extensive fragmentation of all N–C_α bonds. In contrast, ETD of the doubly protonated melectin peptide specifically cleaves N–C_α bonds near the N and C termini. These dissociations can be correlated with unpaired electron distribution in amide π^* orbitals in the vicinity of lysine ammonium groups in peptide cation-radicals produced vertically from most stable ion conformers. This interpretation is consistent with the Utah-Washington model of ExD.

EXPERIMENTAL

Materials

The N-terminal decapeptide of melectin was synthesized as described previously[21] and its purity was checked by liquid chromatography and mass spectrometry.

Methods

The peptide was electrosprayed from 50/50/1 methanol/water/acetic acid solutions at about 10 μM concentrations. Electron transfer dissociation (ETD) mass spectra were obtained on a Thermo Fisher Scientific (San Jose (CA), USA) LTQ XL linear ion trap instrument equipped with a chemical ionization source for the production of fluoranthene anions as ETD reagent. Precursor $(M + 2H)^{2+}$ and $(M + 3H)^{3+}$ ions were selected by mass with an isolation width of 3 *m/z* units so as to accommodate nearest ^{13}C isotopologues. The peptide ions were then reacted with fluoranthene anions for 100, 200, 300 and 500 ms. Multiple-stage tandem MS was performed so as to interrogate charge-reduced and fragment ions from ETD. These ETD product ions were selected by mass and collisionally dissociated with the He bath gas at 20% of rf power.

ECD mass spectra were measured on a Thermo LTQ XL 7 T FT Ultra ICR mass spectrometer (LTQ-FT). Precursor $(M + 2H)^{2+}$ and $(M + 3H)^{3+}$ ions were isolated in the linear trap quadrupole with a 3.3 and 2.7 *m/z* unit mass selection window, respectively, then transferred to the ion cyclotron resonance cell where they were irradiated by free electrons from an external source. The irradiation pulse width was varied between 20 and 500 ms, and the electron emitter bias was set at a nominal potential value of 3 or 5V. Sixty scans were collected and averaged for the *m/z* 50–1150 mass range. The flow rate in the ECD and ETD measurements was typically 1 ul/min.

Computations

Molecular dynamics calculations were performed using NAMD [30]. Initial valence bond structures were created for two series of doubly charged ion tautomers that were protonated either at the ε-amino groups of both lysine residues or at the N-terminal amino group and the ε-amino group of the Lys_8 residue. The molecular parameters for amino acid residues and charged groups used established values from the CHARMM force-field[31]. Replica exchange molecular dynamics[32] (REMD) calculations were performed on each peptide ion tautomer. Calculations were run for 10 ns with a step size of 1 fs with 8 temperature replicas from 300 to 800 K. An amount of 1000 structures from each replica were selected at regular intervals for a total of 8000 initial candidate structures. The temperature interval was chosen to provide sufficient kinetic energy for conformer equilibration but prevent undesirable cis-trans amide bond isomerizations. Each candidate structure was then optimized with PM6 [33] using Gaussian 09 [34]. The PM6 optimized structures were then analyzed for potential hydrogen bonds. Structures with the same hydrogen bonds were grouped together and the lowest energy structure from each group was taken to form a new list of candidate structures. Attempts at reoptimization of several PM6-optimized structures using B3LYP/6-31+G(d,p)[35] were unsuccessful because of persistent convergence failures that occurred at intermediate optimization steps. These failures of B3LYP for these large molecular systems may be connected to the known problem of electron self interaction that occurs because of a slow decay of exchange-correlation potentials[23]. Therefore, a single point energy for each candidate structure was calculated with B3LYP and the 6-31++G(2d,p) and 6-311+G(2d,p) basis sets, and used for initial energy ranking. The lowest energy structures were then used as geometry guesses for optimization with the Coulomb-attenuated hybrid functional (cam-B3LYP)[23] and the 6-31+G(d,p) basis set. Because of the large size of these systems and slow convergence of cam-B3LYP calculations, the optimizations were terminated when the predicted energy change dropped below 10^{-5} a.u. (0.026 kJ/mol), which typically occurred after 50 geometry

optimization cycles. Single point calculations were performed for charge-reduced ions using UB3LYP or ωB97x [24] and the 6-31++G(2d,p) basis set. Atomic charge and spin densities were calculated using Natural Population Analysis[36].

Thanks are due to Dr. Priska von Haller of the University of Washington Proteomics Resource Center for access to the Thermo LTQ XL instrument. Research support by the National Science Foundation (Grants CHE-0750048 for experiments and CHE-0342956 for computations) is gratefully acknowledged. The Department of Chemistry Computer Facility has been jointly supported by the NSF and University of Washington.

REFERENCES

1. Hakansson K., Klassen J. S.: *Electrospray and MALDI Mass Spectrometry*, 2nd ed., pp. 571–630. Wiley, New York 2010.
2. Syka J. E. P., Coon J. J., Schroeder M. J., Shabanowitz J., Hunt D. F.: *Proc Natl. Acad. Sci. U.S.A.* **2004**, *101*, 9528.
3. Tureček F., Syrstad E. A.: *J. Am. Chem. Soc.* **2003**, *125*, 3353.
4. Tureček F.: *J. Am. Chem. Soc.* **2003**, *125*, 5954.
5. Tureček F., Chen X., Hao C.: *J. Am. Chem. Soc.* **2008**, *130*, 8818.
6. Chung T. W., Tureček F.: *Int. J. Mass Spectrom.* **2011**, doi:10.1016/j.ijms.2010.06.025.
7. Höfner D., Lesko S. A., Binsch G.: *Org. Magn. Res.* **1978**, *11*, 179.
8. Aydin R., Günther H.: *Angew. Chem., Int. Ed. Engl.* **1981**, *20*, 985.
9. Eliel E. L., Wilen S. H.: *Stereochemistry of Organic Compounds*, pp. 688–690. Wiley Interscience, New York 1994,.
10. Tureček F., Panja S., Wyer J. A., Ehlerding A., Zettergren H., Nielsen S. B., Hvelplund P., Bythell B., Paizs B.: *J. Am. Chem. Soc.* **2009**, *131*, 16472.
11. Tureček F.: *J. Mass Spectrom.* **2010**, *45*, 1280.
12. Breuker K., Oh H. B., Horn D. M., Cerda B. A., McLafferty F. W.: *J. Am. Chem. Soc.* **2002**, *124*, 6407.
13. Breuker K., Oh H. B., Lin C., Carpenter B. K., McLafferty F. W.: *Proc. Natl. Acad. Sci. U.S.A.* **2002**, *99*, 15863.
14. Robinson E. W., Leib R. D., Williams E. R.: *J. Am. Soc. Mass Spectrom.* **2006**, *17*, 1469.
15. Mihalca R., Kleinnijenhuis A. J., McDonnell L. A., Heck A. J. R., Heeren R. M. A.: *J. Am. Soc. Mass Spectrom.* **2004**, *15*, 1869.
16. Adams C. M., Kjeldsen F., Zubarev R. A., Budnik B. A, Haselman K. F.: *J. Am. Soc. Mass Spectrom.* **2004**, *15*, 1087.
17. Ben Hamidane H., He H., Tsybin O. Yu., Emmett M. R., Hendrickson C. L., Marshall A. G., Tsybin Y. O.: *J. Am. Soc. Mass Spectrom.* **2009**, *20*, 1182.
18. Patriksson A., Adams C., Kjeldsen F., Raber J., van der Spoel D., Zubarev R. A.: *Int. J. Mass Spectrom.* **2006**, *248*, 124.
19. Skurski P., Sobczyk M., Jakowski J., Simons J.: *Int. J. Mass Spectrom.* **2007**, *265*, 197.
20. Pouthier V., Tsybin Y. O.: *J. Chem. Phys.* **2008**, *129*, 095106/1-095106/11.
21. Čeřovský V., Hovorka O., Cvačka J., Voburka Z., Bednářová L., Borovičková L., Slaninová J., Fučík V.: *ChemBioChem* **2008**, *9*, 2815.
22. a) Roepstorff P., Fohlman, J.: *Biomed. Mass Spectrom.* **1984**, *1*, 601; b) Biemann K.: *Biomed. Environ. Mass Spectrom.* **1988**, *16*, 99.

23. Yanai T., Tew D. P., Handy N. C.: *Chem. Phys. Lett.* **2004**, *393*, 51.
24. Chai J.-D., Head-Gordon M.: *J. Chem. Phys.* **2008**, *128*, 084106-1-15.
25. Chen X., Tureček F.: *J. Am. Chem. Soc.* **2006**, *128*, 12520.
26. Tureček F., Chung T. W., Moss C. L., Wyer J. A., Ehlerding A., Holm A. I. S., Zettergren H., Nielsen S. B., Hvelplund P., Chamot-Rooke J., Bythell B., Paizs B.: *J. Am. Chem. Soc.* **2010**, *132*, 10728.
27. Moss C. L., Chung T. W., Wyer J. A., Nielsen S. B., Hvelplund P., Tureček F.: *J. Am. Soc. Mass Spectrom.* **2011**, *22*, in press.
28. Syrstad E. A., Tureček F.: *J. Am. Soc. Mass Spectrom.* **2005**, *16*, 208.
29. Sobczyk M., Anusiewicz I., Berdys-Kochanska J., Sawicka A., Skurski P., Simons J.: *J. Phys. Chem. A* **2005**, *109*, 250.
30. Phillips J. C., Braun R., Wang W., Gumbart J., Tajkhorshid E., Villa E., Chipot C., Skeel R. D., Kale L., Schulten K.: *J. Comp. Chem.* **2005**, *26*, 1781.
31. MacKerell A. D., Jr., Bashford D., Bellott M., Dunbrack R. L., Jr., Evanseck J. D., Field M. J., Fischer S., Gao J., Guo H., Ha S., Joseph-McCarthy D., Kuchnir L., Kuczera K., Lau F. T. K., Mattos C., Michnick S., Ngo T., Nguyen D. T., Prodhom B., Reiher III W. E., Roux B., Schlenkrich M., Smith J. C., Stote R., Straub J., Watanabe M., Wiorkiewicz-Kuczera J., Yin D., Karplus M.: *J. Phys. Chem. B* **1998**, *102*, 3586.
32. Sugita Y., Okamoto Y.: *Chem. Phys. Lett.* **1999**, *314*, 141.
33. Stewart J. J. P.: *J. Mol. Model.* **2007**, *13*, 1173.
34. Frisch M. J., Trucks G. W., Schlegel H. B., Scuseria G. E., Robb M. A., Cheeseman J. R., Scalmani G., Barone V., Mennucci B., Petersson G. A., Nakatsuji H., Caricato M., Li X., Hratchian H. P., Izmaylov A. F., Bloino J., Zheng G., Sonnenberg J. L., Hada M., Ehara M., Toyota K., Fukuda R., Hasegawa J., Ishida M., Nakajima T., Honda Y., Kitao O., Nakai H., Vreven T., Montgomery J. A., Jr., Peralta J. E., Ogliaro F., Bearpark M., Heyd J. J., Brothers E., Kudin K. N., Staroverov V. N., Kobayashi R., Normand J., Raghavachari K., Rendell A., Burant J. C., Iyengar S. S., Tomasi J., Cossi M., Rega N., Millam J. M., Klene M., Knox J. E., Cross J. B., Bakken V., Adamo C., Jaramillo J., Gomperts R., Stratmann R. E., Yazyev O., Austin A. J., Cammi R., Pomelli C., Ochterski J. W., Martin R. L., Morokuma K., Zakrzewski V. G., Voth G. A., Salvador P., Dannenberg J. J., Dapprich S., Daniels A. D., Farkas O., Foresman J. B., Ortiz J. V., Cioslowski J., Fox D. J.: *Gaussian 09*, Revision A.02. Gaussian, Inc., Wallingford (CT) 2009.
35. a) Becke A. D.: *J. Chem. Phys.* **1993**, *98*, 1372; b) Becke A. D.: *J. Chem. Phys.* **1993**, *98*, 5648; c) Stephens P. J., Devlin F. J., Chabalowski C. F., Frisch M. J.: *J. Phys. Chem.* **1994**, *98*, 11623.
36. Reed A. E., Weinstock R. B., Weinhold F.: *J. Chem. Phys.* **1985**, *83*, 735.